



Search for $H \rightarrow WW$ Production with Leptons and Hadronic Taus in the Final State Using 9.7 fb^{-1}

The CDF Collaboration
URL <http://www-cdf.fnal.gov>
(Dated: February 22, 2012)

We present the results of the CDF search for a Standard Model Higgs boson decaying into a pair of W bosons with electrons, muons and hadronically decaying taus in the final state. In particular, we investigate two experimental signatures: a channel with an electron or muon plus a tau, which is mainly sensitive to the Higgs boson direct production via $gg \rightarrow H$, and a channel with two leptons and a tau, which is sensitive to the Higgs boson production in association with a W or Z electroweak boson.

In the full CDF Run II dataset, which amounts to 9.7 fb^{-1} of data, we expect 803 ± 128 background events in the $e\tau$ channel and 625 ± 91 events in the $\mu\tau$ channel and 1.42 ± 0.17 and 1.09 ± 0.12 signal events, respectively, for a Higgs mass of $160 \text{ GeV}/c^2$. In data we observe 789 $e\tau$ events and 597 $\mu\tau$ events. In the case of the $\ell\ell'\tau$ channel, we expect 40.0 ± 5.4 background events and 0.54 ± 0.05 signal events for a Higgs mass hypothesis of $160 \text{ GeV}/c^2$, whereas in data we count 28 events.

We combine the three channels and set a 95% C.L. upper limit on $\sigma/\sigma_{\text{SM}}$ of 10.4 for a Higgs mass hypothesis of $160 \text{ GeV}/c^2$. The expected 95% C.L. upper limit for the same mass is 8.7. Results for other nineteen Higgs mass hypotheses ranging from $110 \text{ GeV}/c^2$ to $200 \text{ GeV}/c^2$ are also presented.

I. INTRODUCTION

The Higgs mechanism is introduced in the Standard Model to explain the electroweak symmetry breaking and the origin of boson and fermion masses. Current precision electroweak measurements constrain the mass of a standard model Higgs boson to be less than $161 \text{ GeV}/c^2$ (one-sided 95% C.L. upper limit) or $185 \text{ GeV}/c^2$ when including the LEP-2 direct search lower bound limit of $114.4 \text{ GeV}/c^2$ at 95% C.L [1].

In this note we report on the results of the CDF searches for $H \rightarrow WW^* \rightarrow \ell\nu_\ell \tau\nu_\tau$, where $\ell = e, \mu$, $WH \rightarrow WWW^* \rightarrow \ell\nu_\ell \ell'\nu_{\ell'} \tau\nu_\tau$, where $\ell, \ell' = e, \mu$, and $ZH \rightarrow ZWW^* \rightarrow (\ell)\ell \ell'\nu_{\ell'} \tau\nu_\tau$, where $\ell, \ell' = e, \mu$ and one of the leptons is not detected. We use 9.7 fb^{-1} of data, produced by the Tevatron collider at $\sqrt{s} = 1.96 \text{ TeV}$, which correspond to the full dataset collected by the CDF detector in Run II.

The analysis is based on events with one or two fully identified leptons of first or second generation and one fully identified hadronically decaying τ . In the following we will refer to the two cases as $\ell\tau$ and $\ell\ell'\tau$ channels. A minimal event selection is applied to reduce the background while maintaining a large fraction of the signal. In order to increase the sensitivity of the search a Boosted Decision Tree (BDT) [2] is used to further discriminate the signal from the background. The BDT uses both event kinematics and τ identification observables and is trained for nineteen Higgs mass hypotheses ranging from 110 to 200 GeV/c^2 . A Bayesian method is used to calculate a 95% C.L. upper limit on the Higgs production cross section based on the predicted and observed distributions of the BDT outputs.

II. DETECTOR DESCRIPTION

The components of the CDF II detector relevant to this analysis are described briefly here; a more complete description can be found elsewhere [3]. The detector geometry is described by the azimuthal angle φ and the pseudo-rapidity $\eta = -\ln(\tan\vartheta/2)$, where ϑ is the polar angle of a particle with respect to the proton beam axis (positive z -axis). The pseudo-rapidity of a particle originating from the center of the detector is referred to as η_{det} . The trajectories of charged particles are reconstructed using silicon micro-strip detectors [4, 5] and a 96-layer open-cell drift chamber (COT) [6] embedded in a 1.4 T solenoidal magnetic field. For $|\eta_{\text{det}}| \leq 1$, a particle traverses all 96 layers of the COT; this decreases to zero at $|\eta_{\text{det}}| \approx 2$. The silicon system provides coverage with 6 (7) layers with radii between 2.4 cm and 28 cm for $|\eta_{\text{det}}| < 1$ ($1 < |\eta_{\text{det}}| < 2$). Outside of the solenoid are electromagnetic (EM) and hadronic (HAD) sampling calorimeters segmented in a projective tower geometry. The first hadronic interaction length (λ) of the calorimeter, corresponding to 19-21 radiation lengths (X_0), uses lead absorber for measuring the electromagnetic component of showers, while the section extending to 4.5-7 λ uses iron to contain the hadronic component. The calorimeters are divided in a central ($|\eta_{\text{det}}| < 1$) and forward ($1.1 < |\eta_{\text{det}}| < 3.64$) region. Shower maximum detectors (SMX) embedded in the electromagnetic calorimeters at approximately 6 X_0 help in the position measurement and background suppression for electrons. Outside of the central calorimeters are scintillators and drift chambers for identifying muons as minimum ionizing particles.

III. LEPTON IDENTIFICATION

The data are collected with inclusive high- p_T lepton (electron or muon) triggers. We use the same data samples and the same lepton selection as the search for a Higgs boson decaying to two W bosons with leptons in the final state [7].

All electrons and muons are required to be isolated such that the sum of the E_T for the calorimeter towers in a cone of $\Delta R = \sqrt{(\Delta\eta)^2 + (\Delta\varphi)^2} < 0.4$ around the lepton is less than 10% of the electron E_T or muon p_T . The transverse energy E_T of a shower or calorimeter tower is $E \sin\vartheta$, where E is the associated energy. Similarly, p_T is the component of the track momentum transverse to the beam line.

Electron candidates are required to have a ratio of HAD energy to EM energy consistent with originating from an electromagnetic shower. The candidate electron has to be associated to a well-measured track satisfying $p_T > 10 \text{ GeV}/c$ that is fiducial to the central shower maximum detector (SMX) and matched to a central EM energy cluster. The candidate is also required to have a matching cluster in the SMX, minimal energy sharing between towers, and a ratio for shower energy E to track momentum p of less than $2.5 + 0.0015 E_T$.

Muons are identified by a charged track releasing a small amount of energy in the calorimeter and matched to a reconstructed track segment (“stub”) in the muon chambers. For $|\eta_{\text{det}}| < 1.2$, strict requirements on the number of tracking chamber hits and the χ^2 of the track fit are placed on the muon tracks in order to suppress kaon decay-in-flight backgrounds. In order to suppress the background from cosmic rays, the track point of closest approach to the beamline must be consistent with originating from the beam line.

Component	$e\tau$	$\mu\tau$
dijet, $\gamma + \text{jet}$	0 ± 34	0 ± 29
$Z \rightarrow \tau\tau$	0.5 ± 0.2	1.2 ± 0.8
$Z \rightarrow \ell\ell$	14.4 ± 3.6	78 ± 12
W+jets	745 ± 123	513 ± 85
$W\gamma$	2.5 ± 0.4	2.3 ± 0.4
Diboson (WW, WZ, ZZ)	24.8 ± 3.7	19.4 ± 2.9
$t\bar{t}$	15.5 ± 2.6	11.2 ± 1.8
Total bkg	803 ± 128	625 ± 91
$gg \rightarrow H$ [$m_H = 160$]	0.96 ± 0.16	0.75 ± 0.12
WH [$m_H = 160$]	0.225 ± 0.031	0.166 ± 0.023
ZH [$m_H = 160$]	0.144 ± 0.020	0.107 ± 0.015
VBF [$m_H = 160$]	0.087 ± 0.014	0.067 ± 0.011
Total signal	1.42 ± 0.17	1.09 ± 0.12
Data	789	597

TABLE I: Yields in the $e\tau$ and $\mu\tau$ channels (signal region). The total errors are quoted.

The tau hadronic decays typically contain charged pions, neutral pions, and a tau neutrino. Since the decay products are collimated, a “signal” cone around a good quality track with $p_T > 10$ GeV/c is defined as $\alpha_{\text{sig}} = \min(0.17, 5/E^{\text{clu}} [\text{GeV}])$ rad, where E^{clu} is the calorimeter energy of the candidate tau. Charged pions are reconstructed as tracks in the signal cone while neutral pions as calorimeter showers. In particular, the search is based on τ 's with either one (1-prong) or three (3-prong) tracks such that the sum of the charges is ± 1 . Since the neutrino escapes detection, only a partial reconstruction of the tau momentum is possible. A so called “visible momentum” is defined as the sum of the track momenta and neutral pion momenta in the signal cone. To be identified, τ 's must exhibit $E_T^{\text{vis}} > 15$ (20) GeV for 1-prong (3-prong) candidates. To suppress the large contamination from jets, the visible mass is requested to be smaller than 1.8 (2.2) GeV/ c^2 for 1-prong (3-prong) candidates. Muons mis-reconstructed as taus are rejected by imposing the ratio of energy to momentum to be larger than 0.8. Electrons are separated from taus using the relation between the electromagnetic fraction and the total calorimeter energy associated to the candidate: $\frac{E_{\text{tot}}}{\sum |\vec{p}|} (0.95 - E_{\text{em}}/E_{\text{tot}}) > 0.1$. Finally the following are the criteria for isolation, based on the “isolation” cone $\min(0.17, 5/E^{\text{clu}} [\text{GeV}]) < \alpha_{\text{iso}} < 0.52$ rad:

- track isolation, defined as the scalar sum of the p_T 's of all tracks with $p_T > 1$ GeV/ c^2 in the isolation cone: $I_{\text{trk}} < 2$ GeV/ c ;
- no tracks with $p_T > 1.5$ GeV/ c in the isolation cone;
- π^0 isolation, defined as the sum of the E_T 's of all π^0 's with $E_T > 1$ GeV reconstructed in the isolation cone: $I_{\pi^0} < 1$ GeV.

The details about τ identification are documented in [8].

To identify the presence of neutrinos, we use the missing transverse energy $\cancel{E}_T = |\sum_i E_{T,i} \hat{n}_{T,i}|$, where the $\hat{n}_{T,i}$ is the transverse component of the unit vector pointing from the interaction point to the i -th calorimeter tower. The \cancel{E}_T is corrected for muons which do not deposit completely their energy in the calorimeter.

Candidate events are required to pass one of the online trigger selections implemented in three successively more stringent levels. The final trigger requirements for electrons are an EM energy cluster with $E_T > 18$ GeV matched to a track with $p_T > 8$ GeV/ c , in the central part of the detector, and an EM energy cluster with $E_T > 20$ GeV and $\cancel{E}_T > 15$ GeV, in the forward region where the tracker has not a full coverage. Muon triggers are based on information from muon chambers matched to a track with $p_T > 18$ GeV/ c .

IV. BACKGROUNDS

Several Standard Model processes are expected to pass our event selection and contaminate the data sample, the dominant ones are WW , WZ , ZZ , $t\bar{t}$, $W\gamma$, $Z\gamma$, Z/γ^* and $Z/\gamma^* + \text{jets}$, $W + \text{jets}$. Their geometric and kinematic acceptances are determined using a Monte Carlo (MC) calculation of the $p\bar{p}$ collisions followed by a GEANT3-based simulation of the CDF II detector response [9]. We use the PYTHIA generator [10] to model the WW , WZ , ZZ , $t\bar{t}$, and Drell-Yan (in the case of the $\ell\tau$ channel) processes, whereas for $W\gamma$ and $Z\gamma$ we use the generator described in [11]. The $W + \text{jets}$ and $Z + \text{jets}$ (in the case of the $\ell\ell'\tau$ channel) backgrounds are estimated using the ALPGEN [12] Monte

Component	$\ell\ell\tau$
Z/W + jets	31.6 ± 5.3
$Z + \gamma$	2.6 ± 0.4
Diboson (WW, WZ, ZZ)	3.7 ± 0.7
$t\bar{t}$	2.1 ± 0.4
Total bkg	40.0 ± 5.4
WH [$m_H = 160$]	0.304 ± 0.042
ZH [$m_H = 160$]	0.109 ± 0.015
$gg \rightarrow H$ [$m_H = 160$]	0.092 ± 0.015
VBF [$m_H = 160$]	0.030 ± 0.005
Total signal	0.535 ± 0.048
Data	28

TABLE II: Yields in the $\ell\ell\tau$ signal sample (signal region). The total errors are quoted.

Carlo interfaced with PYTHIA for the showering. We use the leading-order CTEQ5L parton distribution functions (PDFs) to model the momentum distribution of the initial-state partons [13].

The SM backgrounds consist of two categories: events with real leptons and taus and events which contain fake objects, mostly jets which are reconstructed and erroneously identified as hadronic taus. A correction of up to 3% per lepton (electron or muon) is applied to the simulation based on measurements of the lepton reconstruction and identification efficiencies in data using Z decays. The MC τ identification efficiency is corrected at 3% level to match the efficiency in data [8]. In the case of lepton flavor mis-assignment, the MC fake rate is corrected based on the rates measured in data using Z decays. In the case of jets mis-identified as taus, the energy dependent jet $\rightarrow \tau$ rate is corrected in MC according to the rate measured in jet triggered data. Trigger efficiencies are determined from $W \rightarrow e\nu$ data for electrons and from $Z \rightarrow \mu^+\mu^-$ data for muons.

In the $\ell\tau$ channel the background from di-jet and photon-jet production, characterized by two fake objects, is estimated from a data sample of events with two identified leptons with same electric charge. Proper subtraction of electroweak contributions is applied to avoid event over-counting.

V. EVENT SELECTION

The $\ell\tau$ candidates are selected from events with a lepton and a hadronic tau with opposite charge. The electron or muon in the event is required to satisfy the trigger and have $E_T > 20$ GeV ($p_T > 20$ GeV/ c) for electrons (muons). The z -positions of the lepton track and τ seed track at the point of closest approach to the beam-line are required to be within 4 cm of each other. A loose event selection is applied to suppress the various background processes. The invariant mass of the dilepton system is constrained to the range $M_{\tau\ell} > 20$ GeV/ c^2 to reduce the contamination from low mass resonances. Requesting \cancel{E}_T above 20 GeV helps suppressing the Drell-Yan $Z/\gamma^* \rightarrow \ell\ell$, di-jet, and photon-jet processes with \cancel{E}_T due to resolution effects. Drell-Yan $Z/\gamma^* \rightarrow \tau\tau$ events exhibit real \cancel{E}_T and can be rejected if the angle between the \cancel{E}_T and the dilepton transverse momentum is $\Delta\varphi_{\text{dilep}, \cancel{E}_T} > 1.5$ radians. The remaining dominant backgrounds due to WW and W +jets events are partially removed by imposing $\Delta\varphi_{\tau\ell} < 1.5$ radians.

In the $\ell\ell\tau$ channel are selected events with two leptons and one hadronic tau, having total charge ± 1 and originating from the same primary vertex, i.e. the maximum distance in z at the point of closest approach to the beam-line between the leptons and tau tracks must be $|\Delta z_{\text{MAX}}| < 4$ cm. One of the leptons is required to satisfy the trigger selection and have $E_T > 20$ GeV ($p_T > 20$ GeV/ c) for electrons (muons), while the subleading lepton is required to have $E_T > 10$ GeV ($p_T > 10$ GeV/ c) for electrons (muons). The selected events are further requested to have $\cancel{E}_T > 20$ GeV and the invariant mass of same-flavor opposite-sign leptons in the range $20 \text{ GeV}/c^2 < M_{\ell\ell} < 76 \text{ GeV}/c^2$ or $M_{\ell\ell} > 106 \text{ GeV}/c^2$ (Z -mass veto).

The expected and observed yields after the selection cuts are shown in Tabs. I and II for the $\ell\tau$ and $\ell\ell\tau$ channels, respectively.

VI. CONTROL SAMPLES

The background modeling and normalization are tested in several control samples, each of them targeting one specific component. The control samples of the $\ell\tau$ channel are selected as follows:

- W + jets region:

- $M_{\tau\ell} > 20 \text{ GeV}/c^2$, $\cancel{E}_T > 20 \text{ GeV}$, $\Delta\varphi_{\tau\ell} > 2$ radians;
- dijet, photon-jet region:
 - $M_{\tau\ell} > 20 \text{ GeV}/c^2$, $\cancel{E}_T < 20 \text{ GeV}$;
- $Z/\gamma^* \rightarrow \tau\tau$ region:
 - $M_{\tau\ell} > 20 \text{ GeV}/c^2$, $\cancel{E}_T < 20 \text{ GeV}/c^2$, $\Delta\varphi_{\ell, \cancel{E}_T} < 0.5$.

In the $\ell\ell'\tau$ search we define two control samples:

- \cancel{E}_T region:
 - $10 \text{ GeV} < \cancel{E}_T < 20 \text{ GeV}$, Z -mass veto for events with two same-flavor and opposite-charge leptons ($20 \text{ GeV}/c^2 < M_{\ell\ell} < 76 \text{ GeV}/c^2$ or $M_{\ell\ell} > 106 \text{ GeV}/c^2$);
- Z -mass region:
 - $\cancel{E}_T > 20 \text{ GeV}$ and $76 \text{ GeV}/c^2 < M_{\ell\ell} < 106 \text{ GeV}/c^2$, where $M_{\ell\ell}$ is the invariant mass of same-flavor and opposite-charge leptons.

The expected background and the observed data show very good agreement in all the control regions defined in the analysis.

VII. BOOSTED DECISION TREE

Given the large background contamination, advanced statistical techniques ought to be exploited to maximize the sensitivity to the SM Higgs boson production. We used a multivariate technique based on the Boosted Decision Tree. A decision tree is a binary tree classifier based on a set of rectangular cuts applied sequentially to the variables provided as input to the tree. A boosting procedure is applied to enhance the separation performance and make the decision robust against statistical fluctuations in the training samples: new trees are derived from the same training sample by reweighting the events which have been mis-classified. In this way, each tree is extended to a forest of trees and the final decision is taken by a weighted majority vote of the trees in the forest. The BDT structure has been optimized to maximize the signal-background separation: the maximum number of trees is set at 400, the maximum allowed depth for each tree is 5 and each node is required to have at least 400 events. At each node the cut value is optimized by scanning over the variable range with a granularity of 20 steps. We use the Gini index as a separation criterion and apply the adaptive boosting algorithm with a boosting parameter of 0.2.

In the case of the $\ell\tau$ search, the dominant background is the W production when the gauge boson decays into an electron or a muon and an additional jet in the event is mis-identified as a τ . The BDT therefore should aim at discriminating the Higgs signal from such a process with a satisfactory efficiency. The best performance is achieved when the BDT is trained on the $gg \rightarrow H$ signal against the $W + \text{jet}$ background. In particular, the discriminating power is enhanced when event based observables are accompanied by observables specific to the τ identification; the latter help to distinguish real τ leptons from τ candidates originating from jets. The distributions of the variables used as BDT inputs are presented from Figure 1 to Figure 4 in both the $e\tau$ and $\mu\tau$ channels. Examples of signal to background separation and BDT scores for three mass hypotheses are shown in Figure 8 and Figure 9.

In the case of the $\ell\ell'\tau$ channel, the best signal-background separation is obtained when the BDT training is performed on the combined sample of all the signals (WH , ZH , $gg \rightarrow H$, VBF) against the sample of all the backgrounds ($Z/W + \text{jets}$, $Z + \gamma$, dibosons and $t\bar{t}$) with the proper event weights taken into account. The distributions of the variables used as BDT inputs are presented from Figure 5 to Figure 7. Examples of the BDT output distributions for three representative Higgs masses are shown in Figure 10.

VIII. SYSTEMATICS

Systematic uncertainties associated with the Monte Carlo simulation affect the Higgs, WW , WZ , ZZ , $t\bar{t}$, Drell-Yan, $W + \text{jets}$, $Z + \text{jets}$, $W\gamma$ and $Z\gamma$ acceptances taken from the simulated event samples.

Uncertainties originating from lepton selection and trigger efficiency measurements are propagated through the acceptance calculation, giving uncertainties typically of a few percents. The uncertainty due to the τ reconstruction and identification ranges between 1 and 4%, depending on the fraction of real taus in the sample. The fake rate of leptons into τ 's in the $Z/\gamma^* \rightarrow ee/\mu\mu$ sample introduces an uncertainty of the order of 2%. The uncertainty on the jet into τ fake rate affects primarily the $W + \text{jet}$ and $Z + \text{jet}$ samples (9%).

Uncertainty source	WW	WZ	ZZ	tt	$Z \rightarrow \tau\tau$	$Z \rightarrow \ell\ell$	W +jets	$W\gamma$	$gg \rightarrow H$	WH	ZH	VBF
Cross section	6.0	6.0	6.0	10.0	5.0	5.0			14.3	5.0	5.0	10.0
Measured W cross-section							12.0					
PDF Model	1.6	2.3	3.2	2.3	2.7	4.6	2.2	3.1	2.5	2.0	1.9	1.8
Higher order diagrams	10.0	10.0	10.0	10.0	10.0	10.0		11.0		10.0	10.0	10.0
Trigger Efficiency	0.5	0.6	0.6	0.6	0.7	0.5	0.6	0.6	0.5	0.5	0.6	0.5
Lepton ID Efficiency	0.4	0.5	0.5	0.4	0.4	0.4	0.5	0.4	0.4	0.4	0.4	0.4
τ ID Efficiency	1.3	1.6	2.9	2.0	3.3				4.1	2.1	2.2	4.0
Jet into τ Fake rate	5.8	4.8	2.0	5.1		0.1	8.8			4.2	4.0	0.4
Lepton into τ Fake rate	0.2	0.1	0.6	0.2		2.3		2.1	0.05	0.03	0.02	0.04
Luminosity	5.9	5.9	5.9	5.9	5.9	5.9	5.9	5.9	5.9	5.9	5.9	5.9
Total	14.5	14.2	13.9	16.5	13.4	13.7	16.2	13.1	16.2	13.6	13.6	16.0

TABLE III: Systematic uncertainties on the backgrounds and signals for the $e\tau$ (expressed in %).

Uncertainty source	WW	WZ	ZZ	tt	$Z \rightarrow \tau\tau$	$Z \rightarrow \ell\ell$	W +jets	$W\gamma$	$gg \rightarrow H$	WH	ZH	VBF
Cross section	6.0	6.0	6.0	10.0	5.0	5.0			14.3	5.0	5.0	10.0
Measured W cross-section							12.0					
PDF Model	1.5	2.1	2.9	2.1	2.5	4.3	2.0	2.9	2.6	2.2	2.0	2.2
Higher order diagrams	10.0	10.0	10.0	10.0	10.0	10.0		11.0		10.0	10.0	10.0
Trigger Efficiency	1.3	0.7	0.7	1.1	0.9	1.3	1.0	1.0	1.3	1.3	1.2	1.3
Lepton ID Efficiency	1.1	1.4	1.4	1.1	1.2	1.1	1.4	1.2	1.0	1.0	1.0	1.0
τ ID Efficiency	1.3	1.4	1.8	2.0	3.5				4.1	2.1	2.2	4.0
Jet into τ Fake rate	5.8	5.0	4.4	4.4		0.2	8.9			4.5	4.2	0.4
Lepton into τ Fake rate	0.04	0.1	0.1	0.02		2.1		1.2	0.04	0.02	0.02	0.04
Luminosity	5.9	5.9	5.9	5.9	5.9	5.9	5.9	5.9	5.9	5.9	5.9	5.9
Total	14.5	14.3	14.3	16.3	13.4	13.6	16.3	13.0	16.3	13.9	13.8	16.1

TABLE IV: Systematic uncertainties on the backgrounds and signals for the $\mu\tau$ (expressed in %).

Uncertainty source	WW	WZ	ZZ	tt	Z +jets	W +jets	$Z\gamma$	$gg \rightarrow H$	WH	ZH	VBF
Cross section	6.0	6.0	6.0	10.0				14.3	5.0	5.0	10.0
Measured W cross-section						12.0					
Measured Z cross-section					9.7						
PDF Model	2.6	1.9	2.4	1.4	5.4	4.2	4.0	2.4	1.9	1.8	2.1
Higher order diagrams	10.0	10.0	10.0	10.0			11.0		10.0	10.0	10.0
Trigger Efficiency	2.0	2.0	2.0	2.0	2.0	2.0	2.0	2.0	2.0	2.0	2.0
Lepton ID Efficiency	3.1	3.1	3.1	3.1	3.1	3.1	3.1	3.1	3.1	3.1	3.1
τ ID Efficiency	1.3	2.1	1.8	1.1			1.4	4.0	2.2	2.1	3.9
Jet into τ Fake rate	4.2	4.5	4.2	5.1	6.6	6.4	0.07	0.6	3.5	2.9	3.8
Lepton into τ Fake rate	0.6	0.5	0.3	0.2	0.5		0.7	0.08	0.1	0.1	0.07
Luminosity	5.9	5.9	5.9	5.9	5.9	5.9	5.9	5.9	5.9	5.9	5.9
Total	14.5	14.6	14.5	16.7	14.7	15.8	13.9	16.1	13.8	13.7	16.3

TABLE V: Systematic uncertainties on the backgrounds and signals for the $\ell\ell'\tau$ (expressed in %).

We also assign an acceptance uncertainty of 10% due to potential contributions from higher-order effects, which is calculated in a WW sample as the difference between the leading-order (PYTHIA-based [10]) and next-to-leading order (MC@NLO [14]) acceptances.

The acceptance variations due to PDF model uncertainties is assessed to be on the order of a few percents using the 20 pairs of parton distribution functions (PDF) sets described in [15].

The uncertainties on the $WW/WZ/ZZ$ and $t\bar{t}$ cross sections are assigned to be 6% [16] and 10% [17, 18], respectively. Drell-Yan processes have an uncertainty of 5%. We normalize the $W + \text{jets}$ and $Z + \text{jets}$ cross sections to the inclusive W and Z production cross sections measured by CDF [19, 20]. We quote the total systematic error on the measured value as a systematic uncertainty which results in an uncertainty of 12% on the $W + \text{jets}$ estimate. Uncertainties on the theoretical cross sections vary for the different Higgs production mechanisms. Associated production cross sections are known to NNLO, so the theoretical uncertainty on these cross sections is small, less than 5% [21]. Vector Boson Fusion (VBF) production is known only to NLO, so the residual theoretical uncertainty is higher (on the order of 10% [21]). Gluon fusion is a QCD process, so although it is known to NNLO, the corresponding theoretical uncertainty is still significant (14.3%). Further details on the estimation of these uncertainties are provided in [7].

In addition, all signal and background estimates obtained from simulation have a 5.9% uncertainty originating from the luminosity measurement [22].

Tables III, IV and V report the full set of systematics sources estimated for this analysis.

IX. RESULTS

Since no excess is observed above the expected Standard Model backgrounds, the distributions of the BDT outputs are used to set Bayesian 95% C.L. upper limits on the production cross section of the Standard Model Higgs. The 95% C.L. expected limits are determined with a set of 10000 Monte Carlo background-only experiments based on expected yields varied within the assigned systematics. Correlations between the systematics for different backgrounds are taken into account. For each experiment a test statistic is formed from the difference in the likelihood value for the background-only model versus that for the signal plus background model. The results for the $e\tau$, $\mu\tau$ and $\ell\ell'\tau$ channels are presented in Tabs. VI, VII and VIII and Figs. 11, 12 and 13. The combined limits are shown in Table IX and Figure 14.

X. CONCLUSIONS

We performed a search for a Standard Model Higgs boson decaying into a pair of W bosons exploiting the experimental signature with an electron or muon plus a hadronic tau and the signature with two leptons and a hadronic tau in the final state.

In 9.7 fb^{-1} of data we expect 803 ± 128 background events in the $e\tau$ channel and 625 ± 91 events in the $\mu\tau$ channel and 1.42 ± 0.17 and 1.09 ± 0.12 signal events, respectively, for a Higgs mass of $160 \text{ GeV}/c^2$. In data we observe 789 $e\tau$ events and 597 $\mu\tau$ events. In the case of the $\ell\ell'\tau$ channel, we expect 40.0 ± 5.4 background events and 0.54 ± 0.05 signal events for a Higgs mass hypothesis of $160 \text{ GeV}/c^2$, whereas in data we count 28 events.

We combine the three channels and set a 95% C.L. upper limit on $\sigma/\sigma_{\text{SM}}$ of 10.4 for a Higgs mass hypothesis of $160 \text{ GeV}/c^2$. The expected 95% C.L. upper limit for the same mass is 8.7.

Acknowledgments

We thank the Fermilab staff and the technical staffs of the participating institutions for their vital contributions. This work was supported by the U.S. Department of Energy and National Science Foundation; the Italian Istituto Nazionale di Fisica Nucleare; the Ministry of Education, Culture, Sports, Science and Technology of Japan; the Natural Sciences and Engineering Research Council of Canada; the National Science Council of the Republic of China; the Swiss National Science Foundation; the A.P. Sloan Foundation; the Bundesministerium für Bildung und Forschung, Germany; the World Class University Program, the National Research Foundation of Korea; the Science and Technology Facilities Council and the Royal Society, UK; the Institut National de Physique Nucleaire et Physique des Particules/CNRS; the Russian Foundation for Basic Research; the Ministerio de Ciencia e Innovación, and Programa Consolider-Ingenio 2010, Spain; the Slovak R&D Agency; and the Academy of Finland.

-
- [1] The LEP Electroweak Working Group, <http://lepewwg.web.cern.ch/LEPEWWG/>. 2
 - [2] A. Hoecker *et al.*, Proc. Sci **ACAT2007**, 040 (2007); L. Breiman *et al.*, *Classification and Regression Trees*, Wadsworth and Brooks, Monterey, CA, 1984. 2
 - [3] R. Blair *et al.*, The CDF Collaboration, FERMILAB-PUB-96/390-E (1996). 2
 - [4] A. Sill *et al.*, Nucl. Instrum. Methods A **447**, 1 (2000). 2
 - [5] A. Affolder *et al.*, Nucl. Instrum. Methods A **453**, 84 (2000). 2
 - [6] T. Affolder *et al.*, Nucl. Instrum. Methods A **526**, 249 (2004). 2
 - [7] D. Benjamin *et al.*, CDF Public Note 10785 (2012). 2, 7
 - [8] A. Aaltonen *et al.*, The CDF Collaboration, Phys. Rev. Lett. **103**, 201801 (2009). 3, 4
 - [9] R. Brun *et al.*, CERN-DD-78-2-REV, CERN-DD-78-2 3
 - [10] T. Sjostrand, S. Mrenna, P. Skands, Peter, JHEP, **05** 026 (2006) 3, 7
 - [11] U. Baur, E.L. Berger, Phys. Rev. **D47** 4889-4904 (1993) 3
 - [12] M.L. Mangano *et al.*, J. High Energy Phys. **0307** 001 (2003) 3
 - [13] H.L. Lai *et al.*, CTEQ Collaboration, Eur. Phys. J. **C12** 375-392 (2000) 4
 - [14] S. Frixione and B.R. Webber, JHEP 06 (2002), hep-ph/0204244. 7
 - [15] S. Kretzer, H.L. Lai, F.I. Olness, and W.K. Tung, Phys. Rev. **D69**, 114005 (2004). 7
 - [16] J.M. Campbell and R.K. Ellis, Phys. Rev. **D60**, 113006 (1999). 7
 - [17] N. Kidonakis and R. Vogt, Phys. Rev. **D68**, 114014 (2003). 7
 - [18] M. Cacciari, S. Frixione, M.L. Mangano, P. Nason, and G. Ridolfi, JHEP **04**, 068 (2004). 7
 - [19] A. Abulencia *et al.*, J. Phys. G: Nucl. Part. Phys. (2007) 2457-2544. 7
 - [20] T. Aaltonen, *et al.*, Phys. Rev. Lett. 100, 102001 (2008). 7
 - [21] TeV4LHC Working Group, <http://maltoni.home.cern.ch/maltoni/TeV4LHC/SM.html>. 7
 - [22] D. Acosta *et al.*, Nucl. Instrum. Meth. **A494**, 57 (2002). 7

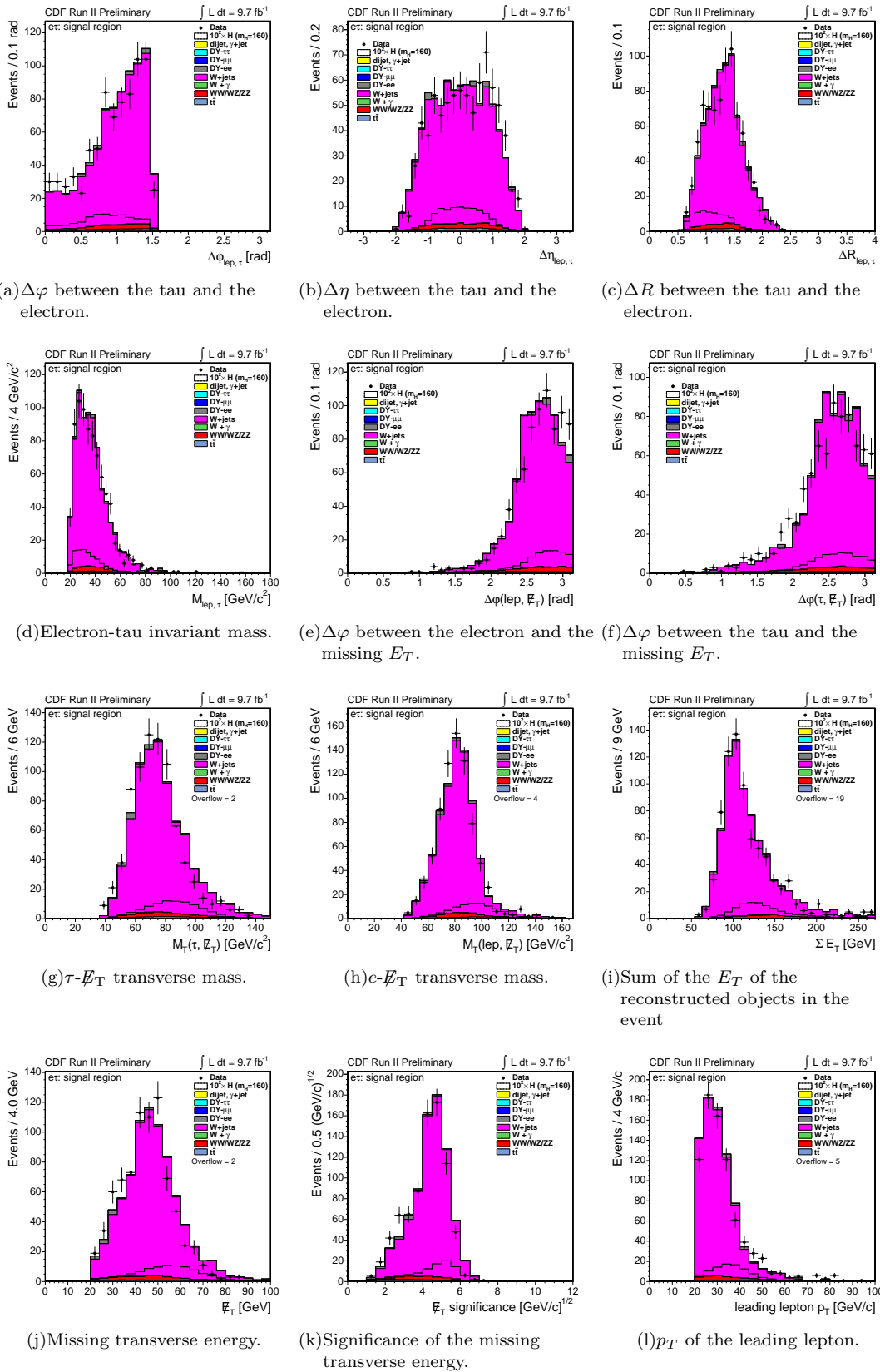


FIG. 1: $e\tau$ channel: data-MC comparison of the variables used in the BDT.

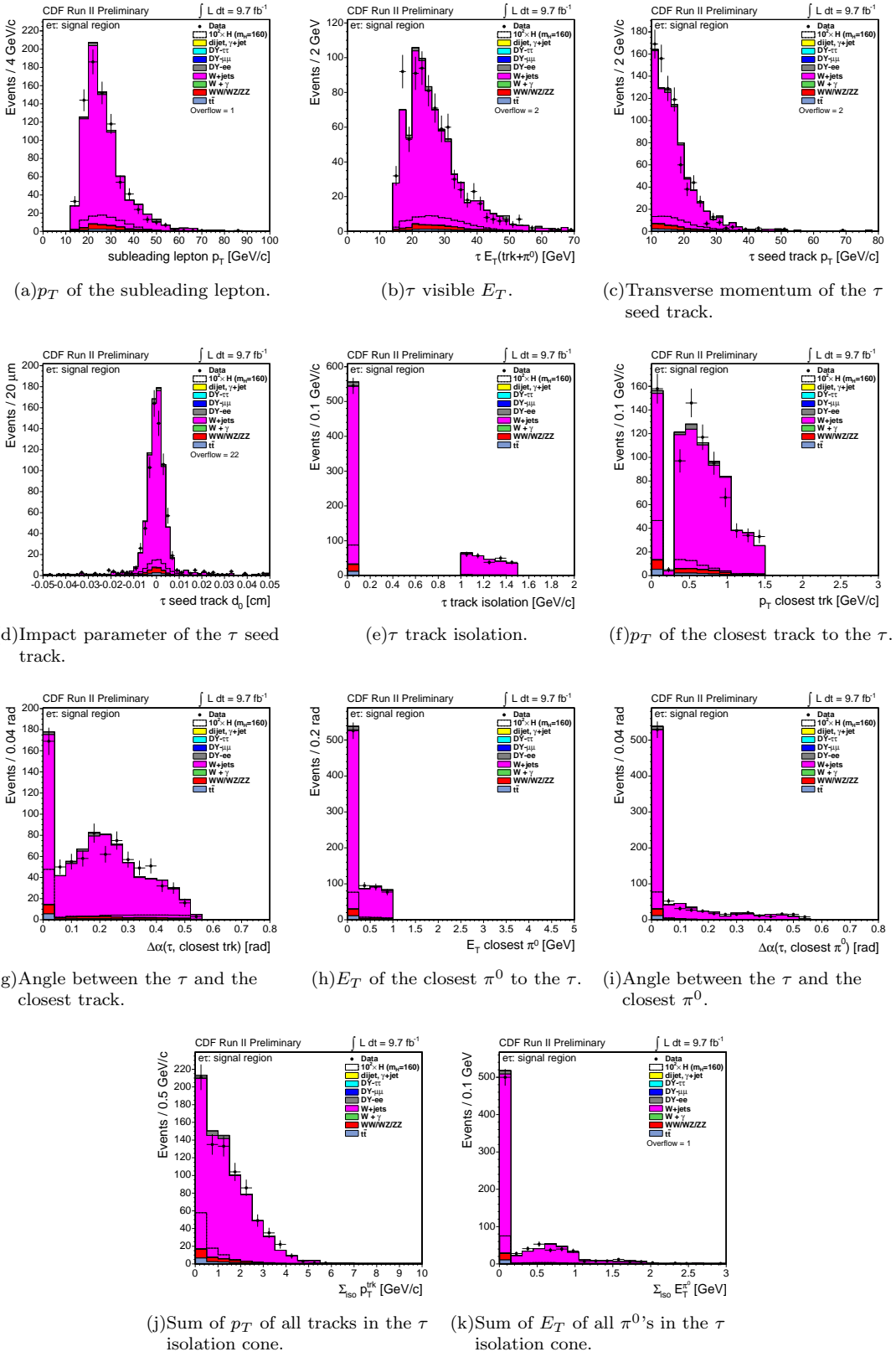


FIG. 2: $e\tau$ channel: data-MC comparison of the variables used in the BDT.

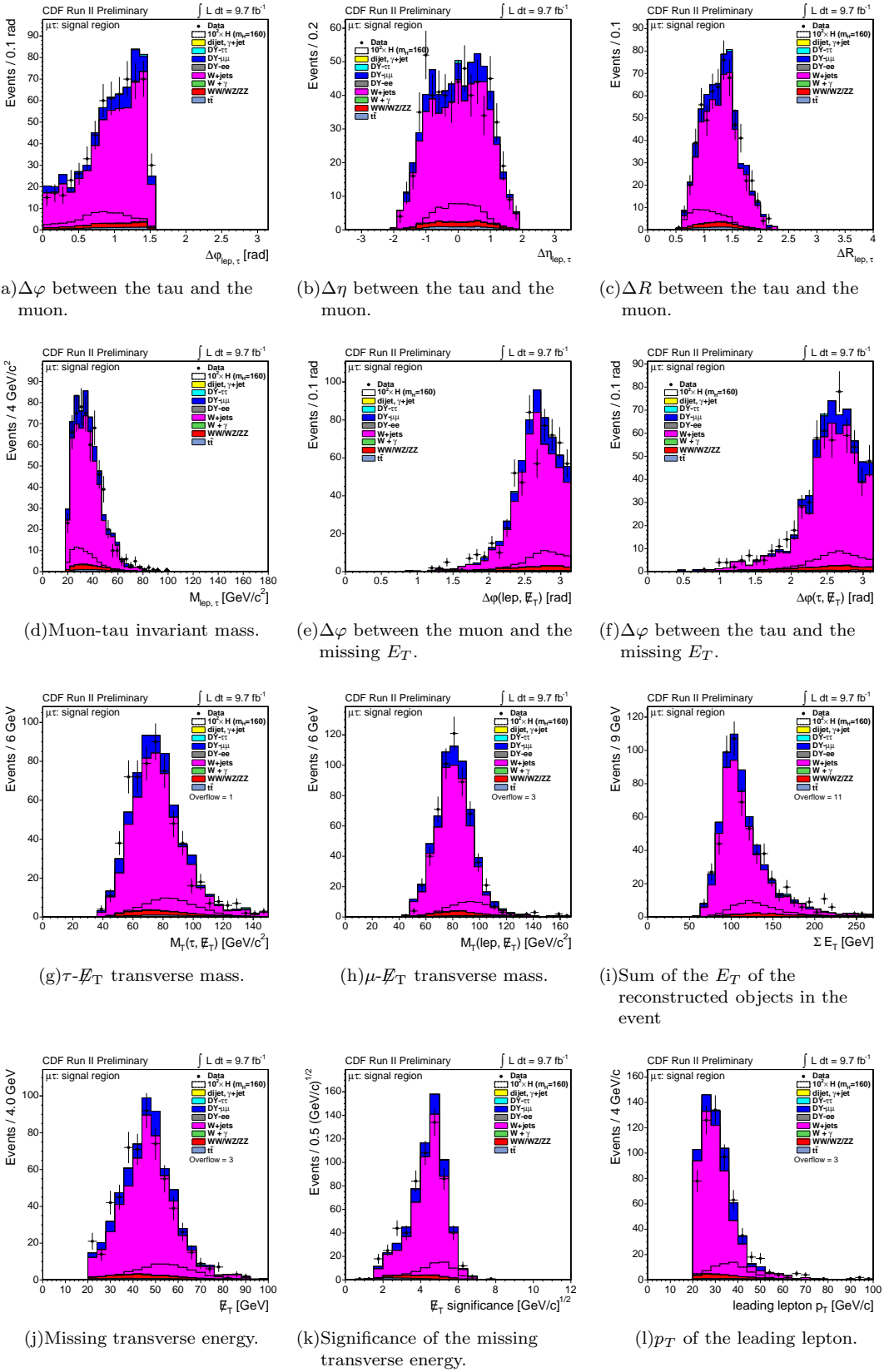
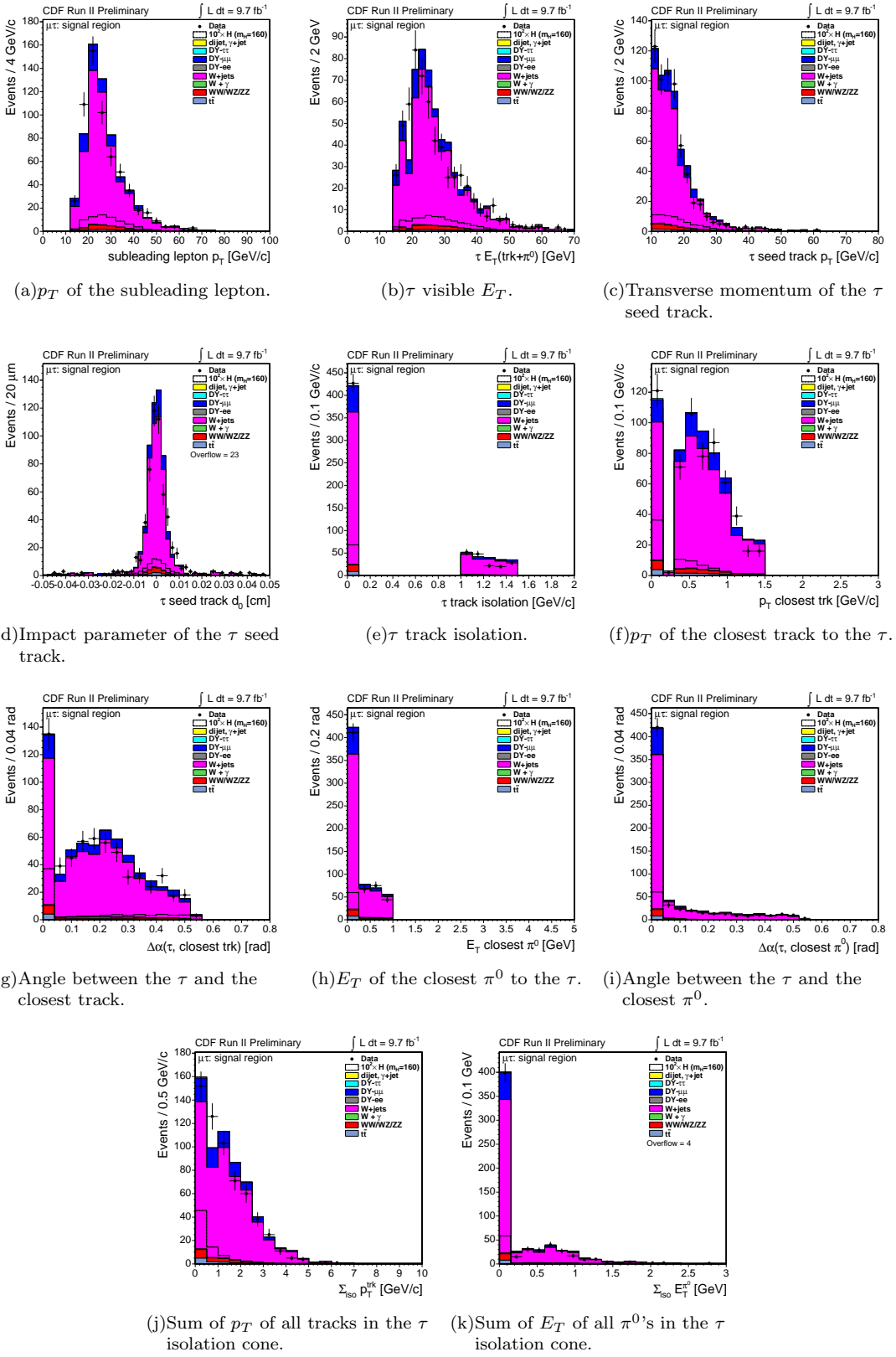


FIG. 3: $\mu\tau$ channel: data-MC comparison of the variables used in the BDT.

FIG. 4: $\mu\tau$ channel: data-MC comparison of the variables used in the BDT.

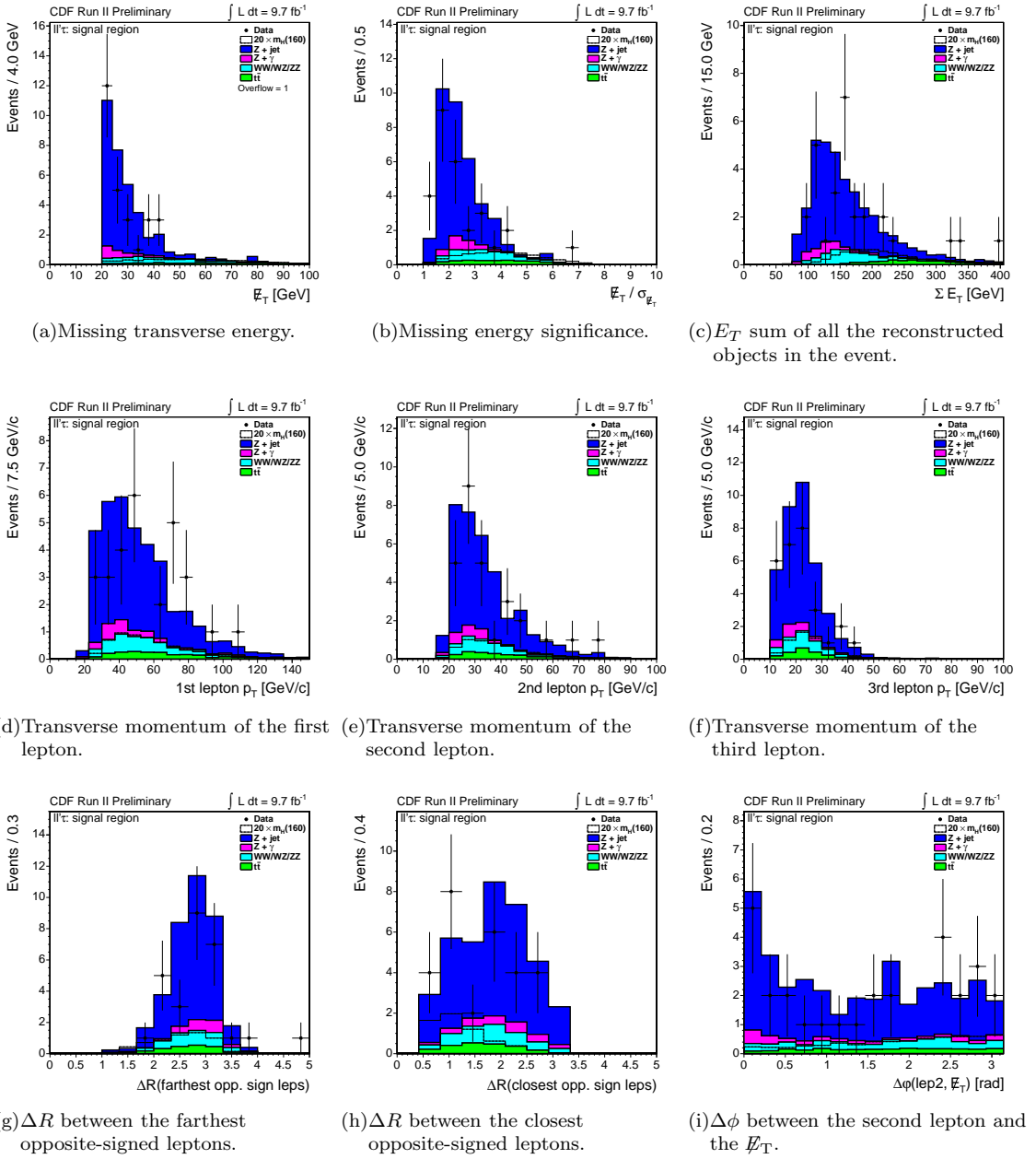


FIG. 5: $\ell\ell'\tau$ channel: data-MC comparison of the variables used in the BDT.

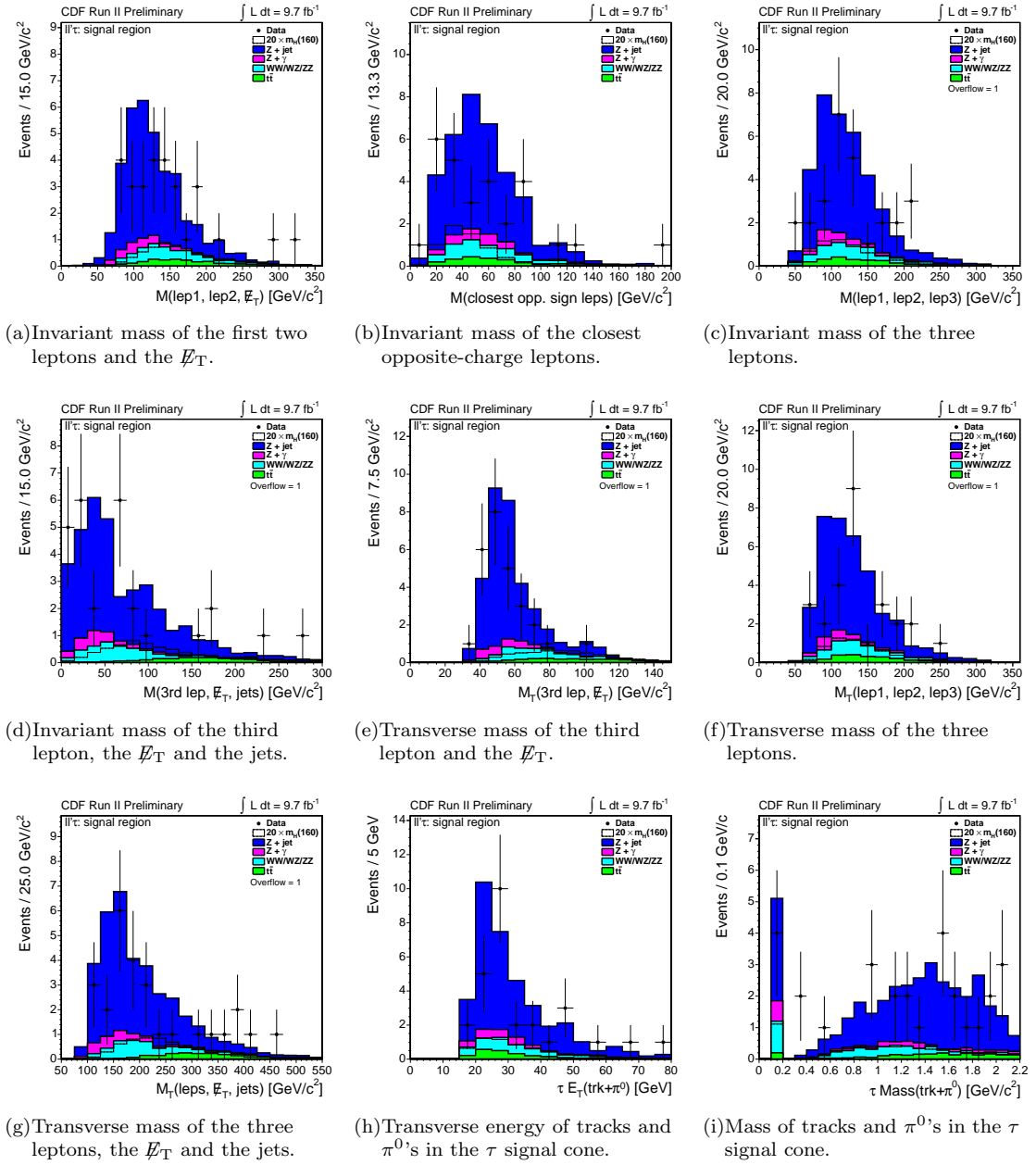


FIG. 6: $\ell\ell'\tau$ channel: data-MC comparison of the variables used in the BDT.

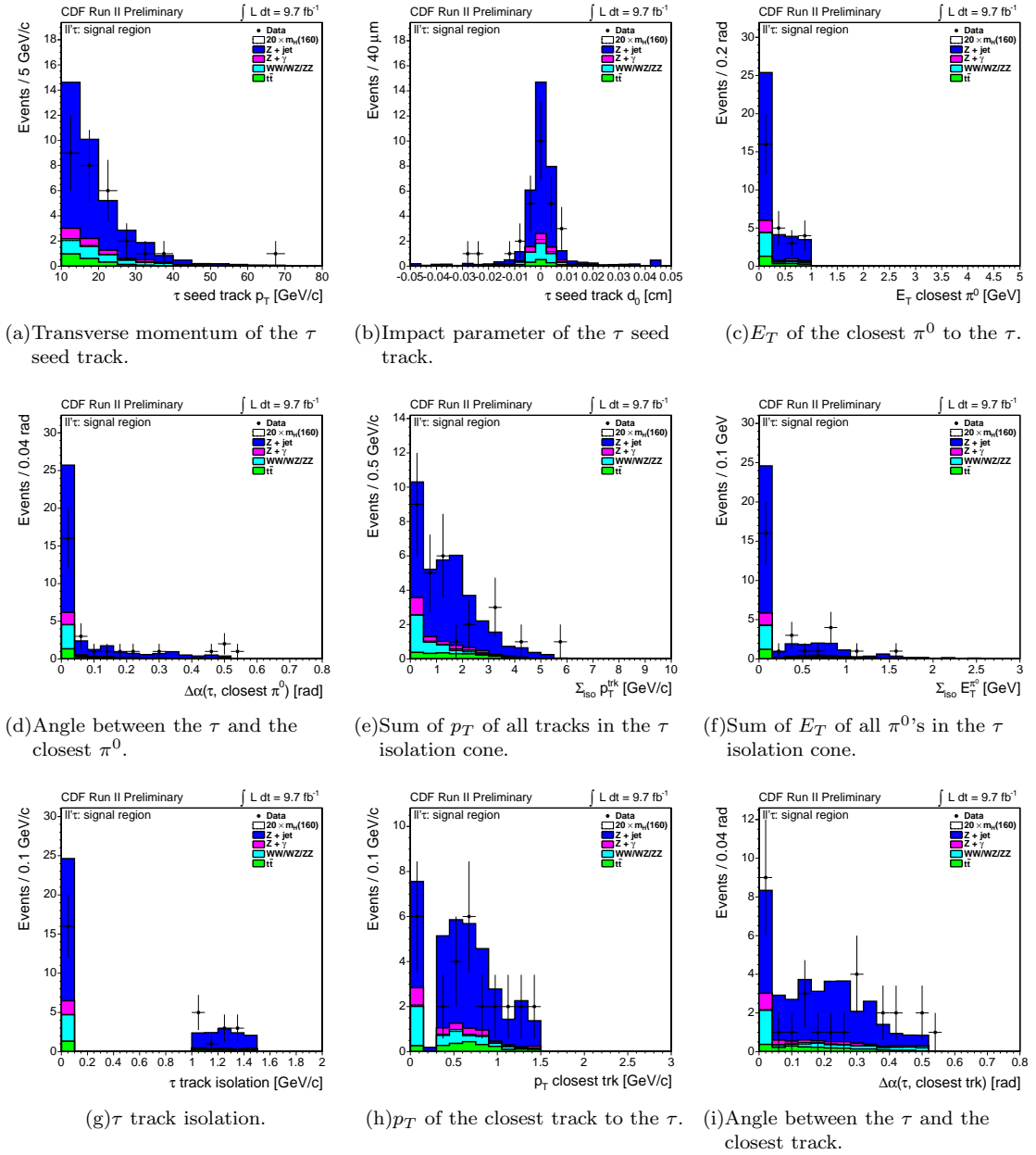


FIG. 7: $ll'\tau$ channel: data-MC comparison of the variables used in the BDT.

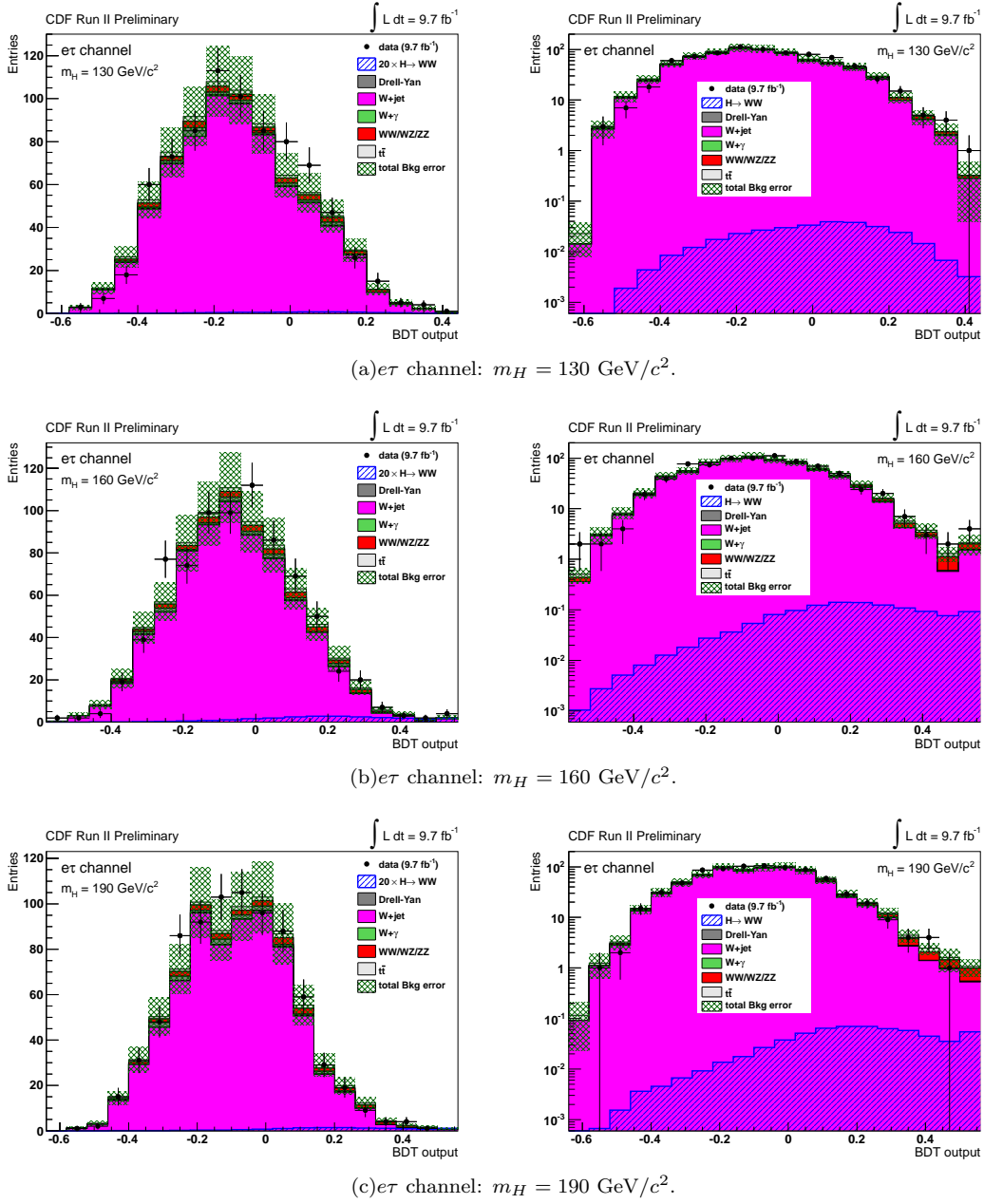


FIG. 8: BDT output distributions for the Higgs mass hypotheses 130, 160, and 190 GeV/c^2 in the $e\tau$ channel.

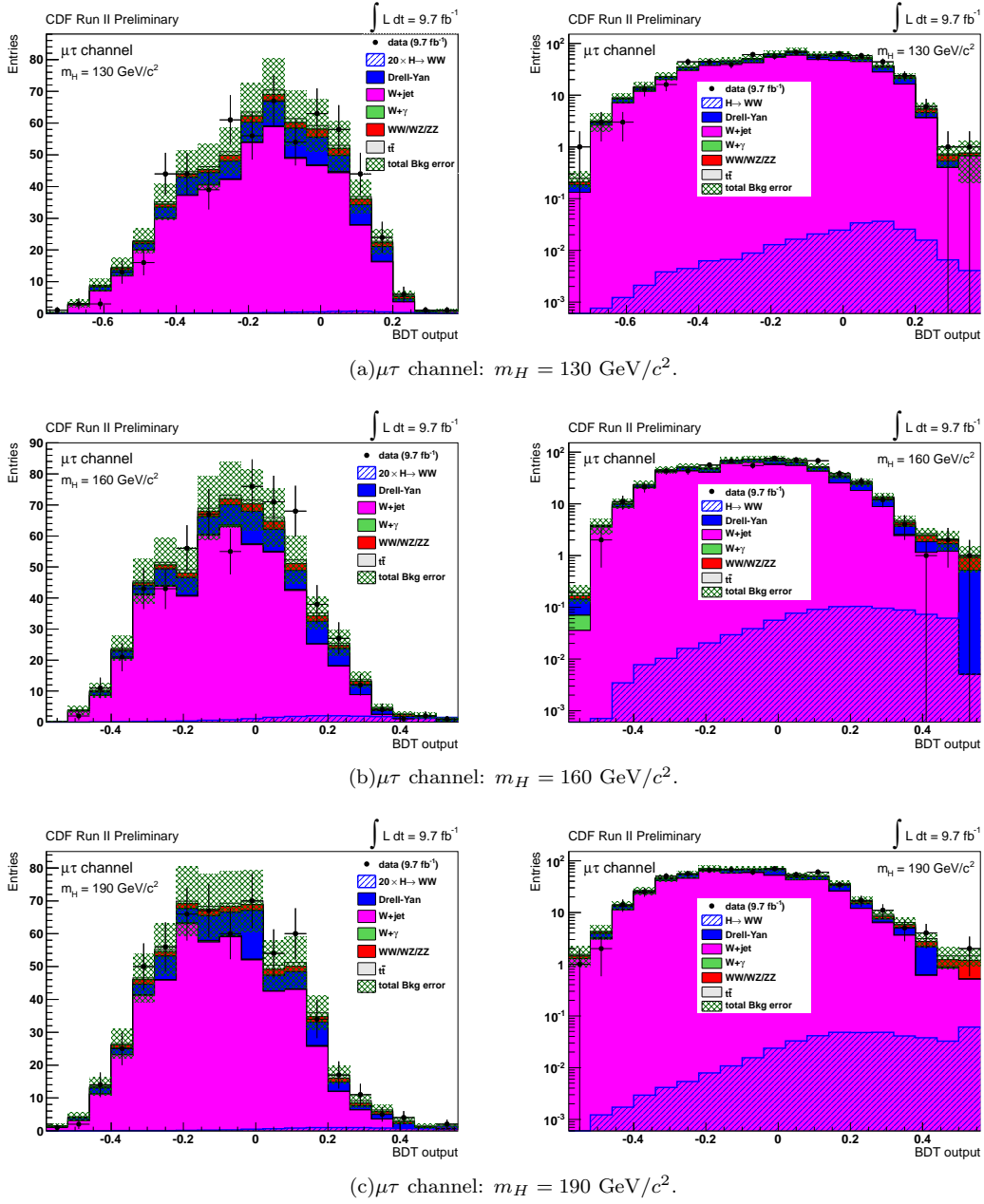


FIG. 9: BDT output distributions for the Higgs mass hypotheses 130, 160, and 190 GeV/c^2 in the $\mu\tau$ channel.

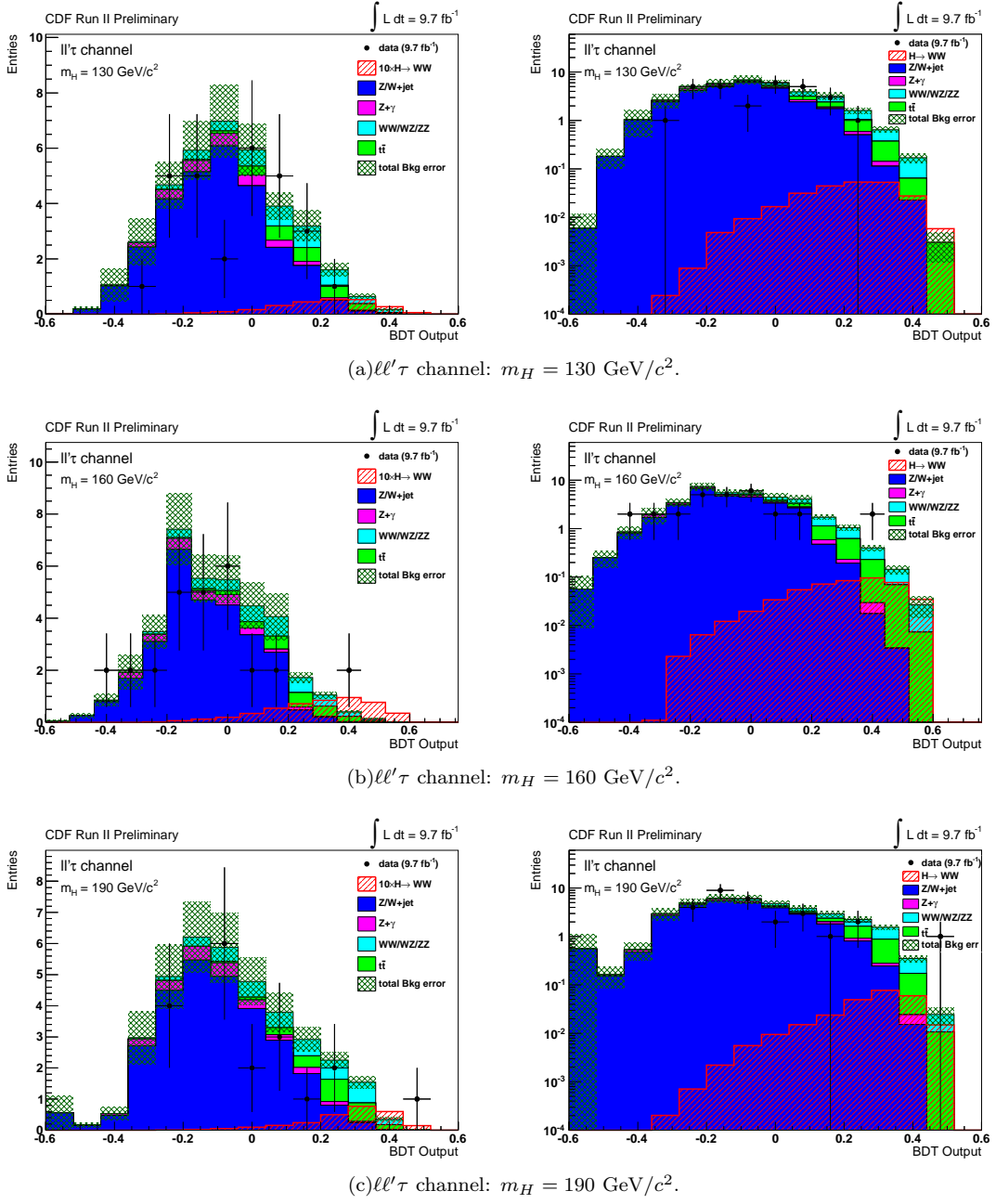
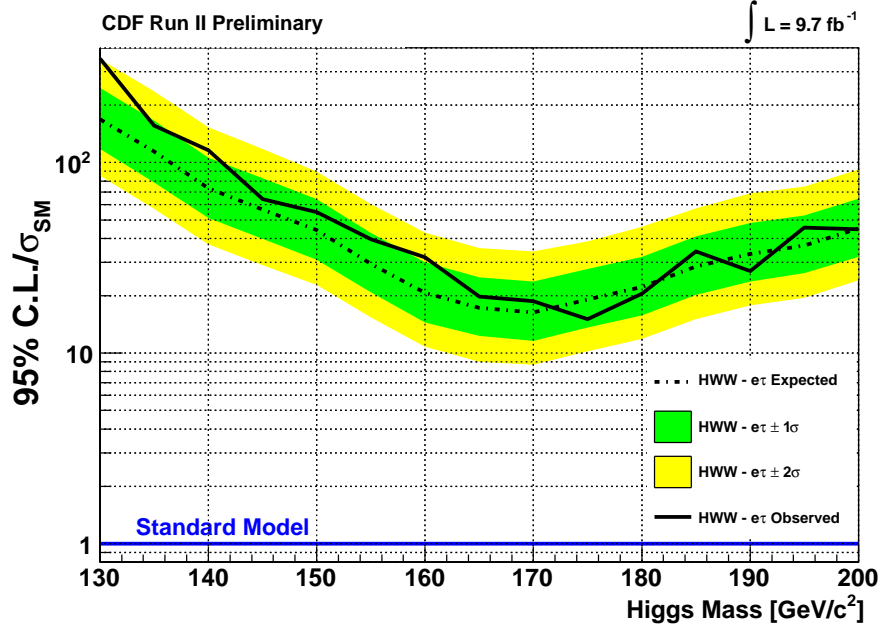
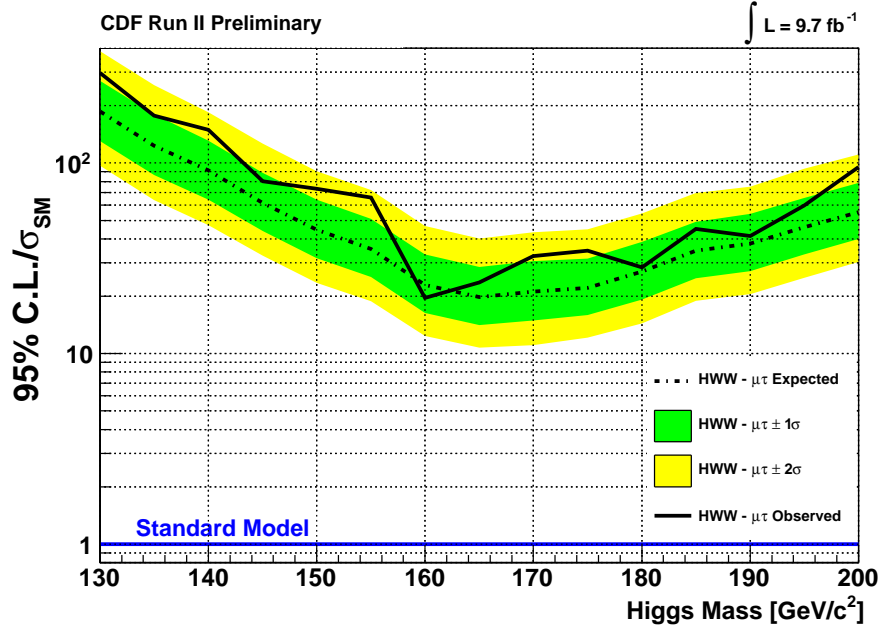


FIG. 10: BDT output distributions for the Higgs mass hypotheses 130, 160, and 190 GeV/c^2 in the $ll'\tau$ channel.

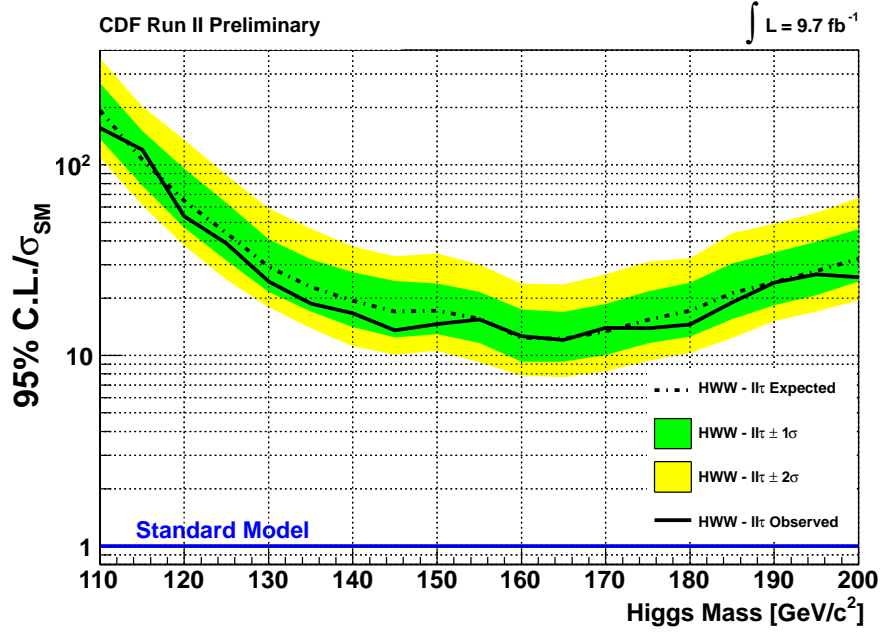
Higgs Mass [GeV/c ²]	-2 σ	-1 σ	Median	+1 σ	+2 σ	Observed
130	85.1	117.6	168.9	245.7	348.7	350.5
135	57.1	78.8	114.3	165.6	236.2	156.4
140	37.3	51.2	73.4	106.0	153.4	115.8
145	28.9	39.7	56.7	82.5	117.8	64.1
150	22.8	30.9	44.3	64.3	89.6	55.0
155	15.4	20.8	29.4	42.6	60.5	39.6
160	10.8	14.5	20.7	30.0	42.8	31.9
165	9.0	12.3	17.3	25.0	35.6	19.8
170	8.7	11.6	16.3	23.8	34.1	18.7
175	10.2	13.6	19.1	27.6	38.5	15.1
180	11.9	15.8	22.2	32.0	45.9	20.5
185	15.1	20.2	28.5	40.9	57.6	34.2
190	17.8	23.8	33.2	48.2	68.8	27.0
195	19.5	26.3	36.7	52.8	74.9	45.5
200	24.1	32.0	45.0	64.5	92.1	44.6

TABLE VI: Estimated and observed limits for the $e\tau$ channel.FIG. 11: Observed and expected limits for the $e\tau$ channel.

Higgs Mass [GeV/c^2]	-2σ	-1σ	Median	$+1\sigma$	$+2\sigma$	Observed
130	96.8	130.1	186.7	270.1	386.3	296.8
135	63.9	86.7	123.3	180.0	257.0	177.0
140	47.2	64.4	91.4	131.1	184.2	149.2
145	32.6	44.1	61.8	88.7	126.3	80.1
150	23.5	31.6	44.7	64.3	90.5	73.2
155	18.8	25.2	35.5	50.8	72.2	65.7
160	12.4	16.4	23.0	33.1	46.6	19.6
165	10.7	14.1	19.8	28.5	40.2	23.6
170	11.1	14.9	21.2	30.5	43.3	32.5
175	12.1	15.9	22.2	31.6	44.9	34.7
180	14.4	19.2	26.9	38.5	54.4	28.4
185	18.9	24.9	34.7	49.1	69.8	45.0
190	20.5	27.1	37.7	54.1	75.3	41.5
195	25.0	33.2	46.0	65.6	93.3	60.0
200	30.3	39.9	55.1	78.5	110.9	95.4

TABLE VII: Estimated and observed limits for the $\mu\tau$ channel.FIG. 12: Observed and expected limits for the $\mu\tau$ channel.

Higgs Mass [GeV/c ²]	-2 σ	-1 σ	Median	+1 σ	+2 σ	Observed
110	108.8	137.2	193.2	268.1	360.7	156.0
115	61.3	77.6	106.4	151.2	203.6	120.1
120	37.8	46.9	65.0	95.5	135.4	53.7
125	25.0	31.5	43.9	63.4	88.1	38.8
130	18.0	21.5	29.2	40.8	59.4	24.4
135	13.9	17.0	23.0	32.0	46.3	18.8
140	11.2	14.1	19.4	27.4	37.4	16.7
145	10.1	12.4	17.0	24.7	33.2	13.5
150	10.6	12.9	17.2	23.9	34.4	14.6
155	9.2	11.7	15.6	21.6	40.0	15.5
160	7.9	9.4	12.4	17.5	23.9	12.6
165	7.7	9.3	12.2	16.9	23.6	12.1
170	8.3	10.0	13.3	18.6	26.7	14.0
175	9.4	11.6	15.4	21.7	31.1	13.9
180	10.3	12.6	17.2	24.1	32.3	14.6
185	12.4	15.6	21.2	30.3	43.7	19.0
190	15.1	18.4	24.2	34.6	49.1	24.1
195	17.0	20.7	27.8	39.5	56.0	26.7
200	19.5	24.4	32.2	46.1	67.3	25.7

TABLE VIII: Observed and expected limits for the $\ell\ell'\tau$ channel.FIG. 13: Observed and expected limits for the $\ell\ell'\tau$ channel.

Higgs Mass [GeV/c ²]	-2 σ	-1 σ	Median	+1 σ	+2 σ	Observed
110	102.8	133.3	183.6	268.0	379.4	163.1
115	56.2	73.3	102.4	148.0	210.4	122.7
120	35.2	45.9	64.2	92.2	132.1	53.3
125	23.0	29.9	41.8	61.2	88.3	39.6
130	15.5	20.3	28.4	40.9	58.2	34.3
135	12.1	15.6	21.7	31.3	44.8	20.7
140	9.4	12.5	17.8	26.3	37.5	21.8
145	8.2	10.8	15.2	22.4	32.1	14.7
150	7.5	10.2	14.3	21.1	30.7	16.4
155	6.2	8.3	11.8	17.3	24.6	18.1
160	4.7	6.2	8.7	12.7	18.1	10.4
165	4.1	5.6	7.9	11.4	16.4	9.4
170	4.3	5.8	8.3	12.2	17.4	11.8
175	4.9	6.6	9.3	13.6	19.5	8.6
180	5.6	7.5	10.8	15.7	22.3	10.0
185	7.2	9.6	13.7	19.8	28.3	14.5
190	8.3	11.1	15.6	22.5	32.3	15.7
195	9.3	12.5	17.8	26.0	36.7	21.8
200	11.1	14.8	21.2	30.7	43.8	23.8

TABLE IX: Combined observed and expected limits for the $e\tau$, $\mu\tau$ and $\ell\ell'\tau$ channels.

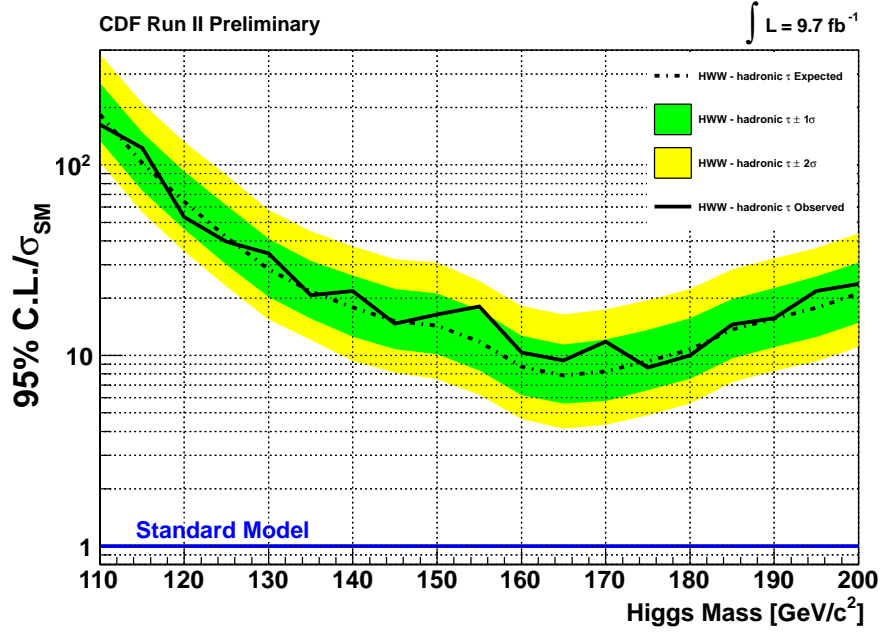


FIG. 14: Combined observed and expected limits for the $e\tau$, $\mu\tau$ and $\ell\ell'\tau$ channels.